NIH Public Access
Author Manuscript
J Am Chem Soc. Author manuscript; available in PMC 2014 August 14.

Published in final edited form as:
J Am Chem Soc. 2013 August 14; 135(32): 11869–11878. doi:10.1021/ja4041779.

Multiplexed Electrochemistry of DNA-bound Metalloproteins

Catrina G. Pheeney, **Anna R. Arnold**, **Michael A. Grodick**, and **Jacqueline K. Barton***
Division of Chemistry and Chemical Engineering, California Institute of Technology, Pasadena, California 91125, USA

Abstract

Here we describe a multiplexed electrochemical characterization of DNA-bound proteins containing [4Fe-4S] clusters. DNA-modified electrodes have become an essential tool for the characterization of the redox chemistry of DNA repair proteins containing redox cofactors, and multiplexing offers a means to probe different complex samples and substrates in parallel to elucidate this chemistry. Multiplexed analysis of EndonucleaseIII (EndoIII), a DNA repair protein containing a [4Fe-4S] cluster known to be accessible via DNA-mediated charge transport, shows subtle differences in the electrochemical behavior as a function of DNA morphology. The peak splitting, signal broadness, sensitivity to π-stack perturbations, and kinetics were all characterized for the DNA-bound reduction of EndoIII on both closely and loosely packed DNA films. DNA-bound EndoIII is seen to have two different electron transfer pathways for reduction, either through the DNA base stack or through direct surface reduction; closely packed DNA films, where the protein has limited surface accessibility, produce electrochemical signals reflecting electron transfer that is DNA-mediated. Multiplexing furthermore permits the comparison of the electrochemistry of EndoIII mutants, including a new family of mutations altering the electrostatics surrounding the [4Fe-4S] cluster. While little change in the midpoint potential was found for this family of mutants, significant variations in the efficiency of DNA-mediated electron transfer were apparent. Based on the stability of these proteins, examined by circular dichroism, we propose that the electron transfer pathway can be perturbed not only by the removal of aromatic residues but also through changes in solvation near the cluster.

INTRODUCTION

Multiplexed electrodes are emerging as a powerful analytical tool particularly in the development of electrochemical diagnostics for the detection of pathogens and cancer markers (1–13). Multiplexed DNA-modified electrodes have been developed to sense an extensive range of targets including small molecule (4, 5, 11), DNA (6, 10, 11, 12), RNA (8, 9, 11), and proteins (3, 7, 11–13). These devices all strive to achieve the same goals of enhanced sensitivity, faster detection times, and tolerance to cell lysates (5, 9, 12). Despite variety in the design of these multiplexed DNA-modified electrodes, they all possess the same intrinsic benefits of statistical comparisons and parallel experimentation; these advantages have proven to be essential for the electrochemical characterization of complex systems. Ultimately, these technologies possess ideal attributes for performing the next generation of fundamental electrochemical measurements as they have been optimized for low variability, real-time monitoring, and complex substrates.

*To whom correspondence should be addressed. jkbarton@caltech.edu.

ASSOCIATED CONTENT

Supporting Information. Primer sequences and experimental procedures. Protein unfolding equation. Figures S1–S4. This material is available free of charge via the Internet at http://pubs.acs.org.

NIH-PA Author Manuscript
NIH-PA Author Manuscript
NIH-PA Author Manuscript

NIH-PA Author Manuscript

NIH-PA Author Manuscript

NIH-PA Author Manuscript

The utility of multiplexed analysis for the fundamental studies of macromolecules was demonstrated in the characterization of charge transport through DNA (12–14). One such case is the measurement of ground state DNA-mediated charge transport (DNA CT) through exceptionally long DNA distances up to 34 nm (14). DNA CT is the process through which charge is conducted through the π-stack of the DNA base pairs (15–17). Both the exquisite sensitivity of even a subtle perturbation in DNA stacking (18,19) and the shallow distance dependence (14,15) of DNA CT have been characterized using DNA-modified electrodes affixed with a redox-active moiety at the distal end of the duplex. Multiplexing these DNA-modified electrodes onto a single device was crucial in establishing that the electrochemical signal was generated via DNA CT over such long molecular distances and that the π-stack of the DNA was well stacked and in a biologically relevant conformation (14).

Here we utilize multiplexed technology to investigate the electrochemistry of DNA repair proteins containing [4Fe-4S] clusters (Figure 1). DNA-modified electrodes have become a necessary tool to investigate the electrochemistry of the iron-sulfur cofactor of many DNA repair proteins, including EndonucleaseIII (EndoIII), MutY, UDG, SoxR, and XPD, towards identifying the *in vivo* relevance for this redox activity (20–24). Upon DNA-binding of EndoIII, the $3^+/2^+$ redox couple of its [4Fe-4S] cluster has been shown to shift ~ −200 mV compared to freely diffusing protein, to approximately 80 mV versus NHE (25). Thus binding of the DNA polyanion brings the $3^+/2^+$ redox potential of the [4Fe-4S] cluster into a physiologically relevant range. Moreover, disease related mutants show deficiencies in DNA CT through their weaker electrochemical signals. Interestingly, DNA–binding proteins involved in genome maintenance have increasingly been found to contain [4Fe-4S] clusters (26–29). We have proposed that the redox chemistry of these [4Fe-4S] clusters are critical as a first step in the search mechanism used by DNA repair proteins to redistribute to the vicinity of DNA damage (21, 30). The proposed model hinges on the ability of these [4Fe-4S] cluster proteins to electronically couple to the π-stack of DNA in order to perform efficient searching of the genome facilitated by DNA CT. This efficient DNA-mediated CT between repair proteins seems to depend on the similar reduction potentials of their clusters. The consistent DNA-bound midpoint potential of these various proteins containing [4Fe-4S] clusters has been of particular interest. In this work, we investigate how the electrostatics of the protein fold, in addition to binding of the DNA polyanion, may tune the reduction potential of the cluster. Thus it becomes important to characterize the DNA-bound electrochemistry of these proteins containing [4Fe-4S] clusters in a quantitative manner that allows for direct side-by-side comparison of potentials and couplings through multiplexing.

EXPERIMENTAL METHODS

Oligonucleotide preparation

All DNA substrates were synthesized on a 3400 Applied Biosystems DNA synthesizer with all phosphoramidites and reagents purchased from Glen Research. The sequences of the DNA substrates used were 5′ - HS –C_6– AGT ACA GTC ATC GCG - 3′ for the thiol strand and 3′ - TCA TGT CAG TAG CGC - 5′ for the complement strand. Additional complements were prepared that yield either a TC mismatch or an abasic site at the position of the underlined adenine. Both the complement and thiol-modified DNA were purified through standard procedures as previously reported (13). All single-stranded DNA was purified by high pressure liquid chromatography (HPLC) using a reverse phase PLRP-S column, purchased from Agilent. The identity of the oligonucleotides was confirmed by matrix-assisted laser-desorption ionization – time of flight (MALDI-TOF) mass spectrometry. The thiol-modified single stranded DNA was reduced with 100 mM dithiothreitol (Sigma) in Tris buffer (50 mM Tris HCl, 50 mM NaCl, pH 8.4) for 40 minutes and purified by size exclusion chromatography (Nap5 Sephadex G-25, GE Healthcare) as well as reverse phase

NIH-PA Author Manuscript

NIH-PA Author Manuscript

NIH-PA Author Manuscript

HPLC. Single-stranded DNA stocks were then desalted by precipitation in ethanol and re-suspended in phosphate buffer (5.0 mM phosphate, 50 mM NaCl, pH 7.0). Equimolar amounts of single-stranded stocks were combined based on quantification by UV-Visible spectroscopy. The extinction coefficients at 260 nm from the IDT SciTools were used for the quantification of the single-stranded DNA stocks. All DNA solutions were then thoroughly deoxygenated with argon and annealed by heating to 90 °C followed by a slow cooling to ambient temperature over 90 minutes.

Site-Directed Mutagenesis

E200K, Y205H and K208E EndoIII mutants were prepared using a pET11 vector containing the *nth* gene with N-terminal ubiquitin and hexahistidine tags (22) and a Quikchange II-E Site-Directed Mutagenesis Kit (Stratagene). Y82A EndoIII was prepared previously (22). Primers were purchased from Integrated DNA Technologies and primer sequences are provided in the Supporting Information (SI). All mutagenized plasmids were sequenced (Laragen) to confirm the desired sequences.

Protein Overexpression and Purification

Mutant and WT pET11 plasmids were transformed into BL21star(DE3)pLysS *E. coli* cells (Invitrogen) for overexpression. The EndoIII proteins were overexpressed and purified according to a protocol adapted from published procedures (22). Notably, it was observed that imidazole destabilized the protein, leading to precipitation. Therefore, imidazole was removed from the HisTrap HP nickel column binding buffer, and a desalting column was used to exchange into an imidazole-free buffer immediately following this column. Additionally, a HiLoad Superdex 16/600 75 pg size exclusion column was used in place of the Superose 12 column. Full protocols for the expression and purification of EndoIII are included in the SI. The glycosylase activity of mutants was compared to that of wild type EndoIII based on previously established methods (22).

Multiplexed Chip Fabrication

Multiplexed chips consisting of 16 gold electrodes were prepared using standard photolithography techniques as adapted from previously established protocols (13). Photoresist was used to pattern nine 1 inch by 1 inch chips on 525 μm thick silicon wafers (SiliconQuest) that had a thermal oxide layer grown to a thickness of roughly 4,000 Å to insulate the wafer. A titanium adhesion layer (3 nm) followed by a gold layer (100 nm) were deposited using an electron beam evaporator without breaking the vacuum between depositions. The metal lift-off was performed directly after metal deposition using Remover PG (MicroChem) heated to 60 °C for one hour. The wafers were then dehydrated by baking at 180 °C for at least 2 hours and an insulating SU8 layer (3 μm) was coated on the wafer. This SU8 layer was patterned such that the working electrodes and contact pads were left exposed yet the connective wires were covered to define a controlled working electrode area (2 mm^2). The SU8 was cured with a final hard bake at 150 °C for 15 minutes. The wafer was then cleaved into individual chips (Dynatex Scriber/Braker) to prevent any scratching of the exposed working electrode surfaces.

DNA-modified Electrode Assembly

Single electrode experiments were performed with a low-volume constrained Au(111) on mica surface (Molecular Imaging), as previously established (20). Multiplexed electrode experiments were performed with the 16 electrode chips divided into four quadrants of four electrodes each (13). Multiplexed chips were cleaned in acetone and isopropanol as well as ozone-cleaned for 5 minutes at 20 mW immediately prior to the assembly into a holder and the exposure to thiol-modified DNA. The cleaned chip was then assembled in a

NIH-PA Author Manuscript

NIH-PA Author Manuscript

NIH-PA Author Manuscript

polycarbonate holder used to position the chip. A rubber gasket and acrylic clamp is used to define the four quadrants and create a common central well. The rubber Buna N gasket (0.020″ thick, unless otherwise indicated) and clamp are manufactured by SAS Industries and Xcentric, respectively. A fresh gasket and clamp are used for each experiment to prevent any cross contamination between experiments.

Duplex DNA (20 μl of 25 μM) was placed in each quadrant of a multiplexed chip and left to self-assemble overnight (16–24 hours) in a humid environment. To ensure efficient monolayer formation, thiol-modified DNA was used within two weeks of the dithiothreitol reduction. Loosely packed DNA films were assembled in the absence of $MgCl_2$ while closely packed DNA films were assembled with the addition of 100 mM $MgCl_2$. Once DNA films were assembled and thoroughly washed with phosphate buffer, the electrodes were backfilled with 1 mM 6-mercaptohexanol (MCH) for 45 min in phosphate buffer with 5 % glycerol. Background scans were acquired with common running buffers exposed to the electrodes. An initial background scan is acquired in phosphate buffer (5 mM phosphate, 50 mM NaCl, pH 7.0) followed by a subsequent scan in spermidine buffer (5 mM phosphate, 50 mM NaCl, 40 mM $MgCl_2$, 5 mM spermidine, pH 7.0).

Protein Electrochemical Measurements

Electrochemical measurements were performed with a CHI620D Electrochemical Analyzer and a 16-channel multiplexer from CH Instruments. A three-electrode setup was used with a common Pt auxiliary and a quasi Ag/AgCl reference electrode (Cypress Systems) placed in the central well of the clamp. Cyclic voltammetry data were collected at 100 mV/s over a window of 0.1 mV to −0.4 mV versus Ag/AgCl unless otherwise indicated. After background scans, EndoIII samples in phosphate buffer (20 mM sodium phosphate, 100 mM NaCl, 0.5 mM EDTA, 20 % glycerol, pH 7.4) were added to the central well or separated quadrants (120 μL total for the four quadrants), ranging in concentrations from 30 – 90 μM quantified using the absorbance of the [4Fe-4S] cluster at 410 nm (ε = 17,000 $M^{-1}cm^{-1}$) (30). EndoIII was allowed to incubate on the multiplexed chip for up to 12 hours and monitored over time. The chip was stored in a humid environment between subsequent scans to prevent solution evaporation and hold the concentration constant over time.

Circular Dichroism Thermal Denaturation

For protein samples (5 μM), the ellipticity at 223 nm (the largest difference between native and denatured protein) was measured as a function of increasing temperature (20 °C to 60 °C) using a Model 62A DS circular dichroism spectrometer (AVIV). All data shown are the average of at least duplicate measurements. Measured ellipticity was converted to fractional change in ellipticity by assigning the native protein a value of 0 and the fully denatured protein a value of 1. In order to extract melting temperature values, data were fit using a non-linear least-squares regression to a simple two-state unfolding model. [32] (see SI) Reported errors in T_m values are derived from this fitting.

RESULTS

Multiplexed electrochemistry of EndoIII

The electrochemical behavior of the [4Fe-4S] cluster of EndoIII incubated on loosely packed DNA films, assembled in the absence of $MgCl_2$, was first compared between individual and multiplexed electrode assemblies. A reversible signal for the [4Fe-4S]-cluster of EndoIII, with the ratio of the reduction and oxidation currents being near unity, at a mid-point potential of 80 ± 3 mV vs. NHE was observed on both single electrode and multiplexed assemblies (Figure 2). The signal size for the redox couple of EndoIII depended on incubation time and concentration on both assemblies; this behavior as well as the mid-

NIH-PA Author Manuscript

NIH-PA Author Manuscript

NIH-PA Author Manuscript

point potential is consistent with previously established results for EndoIII on DNA-modified electrodes (22). The consistency across all 16 multiplexed electrodes was comparable to that seen with previous multiplexed DNA-modified electrodes and showed at most a 3.5 % deviation in signal size (Figure 2) (13). The analogous experiment run on individual single electrodes would yield dramatically higher variability on the order of 20–40 % (22).

Due to the modular nature of the multiplexed electrode assembly, the thickness of the rubber gasket used to seal the central well was varied to increase accessibility to the electrodes. Background scans and EndoIII signal sizes were compared for gaskets 0.064″, 0.032″, and 0.020″ thick. Oxygen contributions in the background scans, likely caused by trapped oxygen in close proximity to the electrode surface, were decreased drastically with the use of the thinner gaskets yielding much more uniform CVs and increased EndoIII signal size (Figure S1). Overall, the most exposed electrodes produced featureless background scan resulting in a 0.020″ thick Buna N gasket being utilized for all subsequent experiments.

EndoIII on differing DNA monolayers

The effect of DNA substrates and film morphology on the EndoIII signal was next investigated. Allowing the self-assembly of DNA monolayers to form in the presence of $MgCl_2$ dramatically affects the film packing and ultimately the density of the DNA monolayer formed (33). In the presence of $MgCl_2$, the negative charge of the DNA phosphate backbone is screened, allowing neighboring duplexes to more closely associate and self-assemble into a tightly packed DNA monolayer.

Incubation of EndoIII on DNA-modified electrodes assembled with duplex DNA (dsDNA) was found to produce a redox couple with the same mid-point potential as previously described (80 ± 3 mV vs. NHE) regardless of DNA film morphology, while single-stranded DNA (ssDNA) monolayers showed cyclic voltammograms that were relatively featureless compared to background scans, even after 8 hours of protein incubation (Figure 3). As both the underlying gold surface and the protein solution were common across all electrodes, this appearance of a reversible redox couple from EndoIII on the dsDNA monolayers but not on the ssDNA films indicates that the signal generated from EndoIII is dependent on binding to duplex DNA. Moreover, since the DNA-bound redox potential for EndoIII is not observed on these ssDNA-modified electrodes, these ssDNA-modified electrodes provide a useful control against surface contaminants.

The DNA-bound signal of EndoIII was then compared on DNA-modified electrodes assembled with different morphologies. The peak splitting for the $3^+/2^+$ redox couple of the [4Fe-4S] cluster of EndoIII was found to be dependent on monolayer morphology, while the mid-point potential remained unaltered. The consistency of the mid-point potentials between the surface morphologies indicates that EndoIII is in the same electrostatic environment, bound to duplex DNA, regardless of the monolayer morphology. The closely and loosely packed DNA monolayers show peak splittings of 88 ± 4 mV and 64 ± 2 mV respectively (Figure 3). In addition to the increase in peak splitting, there is also a broadening of the signal observed upon switching to the more closely packed DNA films. Increases in the peak splitting and broadening of the redox couple are both indicative of decreases in the rate of electron transfer and the homogeneity of the electrochemical process (34). These two characteristics, an increase in peak splitting and heterogeneity, have previously been seen as characteristics of a redox-active moiety on DNA-modified electrodes being reduced by DNA CT (35).

NIH-PA Author Manuscript

NIH-PA Author Manuscript

NIH-PA Author Manuscript

DNA-mediated electrochemistry of EndoIII

The mechanism of electron transfer to the [4Fe-4S] cluster in EndoIII was next investigated on both loosely and closely packed dsDNA-modified electrodes. DNA-mediated reduction is exceptionally sensitive to even subtle perturbations to the intervening π-stack (18, 19). Therefore the yield of [4Fe-4S] cluster reduction was examined after introducing a single perturbation site into the DNA duplexes self-assembled on the electrodes. Either a single thymine-cytosine mismatch (TC) or an abasic site (Ab) were incorporated into thiol-modified dsDNA near the electrode surface to prevent EndoIII binding to the π-stack below the perturbation site, as EndoIII binds non-specifically to non-substrate DNA. The dsDNA stocks for the well-matched (WM), TC, and Ab sequences were all quantified and annealed using the same thiol-modified ssDNA stock. This consistency of the thiol strand avoids any variability caused by the efficiency of monolayer formation due to the reactivity of the thiol-modifier. These dsDNA sequences, as well as a ssDNA control, were then assembled on a multiplexed chip.

The reduction signal for the [4Fe-4S] cluster of EndoIII was characterized across these different DNA substrates on both loosely and closely packed films (Figure 4). When these DNA substrates were assembled in the presence of $MgCl_2$, producing closely packed DNA monolayers, the reduction signal of EndoIII was attenuated upon introducing single base pair lesions. The WM, TC, and Ab dsDNA monolayers gave signal sizes of 56 ± 1 nA, 42 ± 1 nA, and 41 ± 4 nA respectively after EndoIII incubation (60 μM for 8 hours), resulting in an average signal attenuation of 24 ± 1% and 26 ± 2% upon incorporating a TC mismatch or an abasic site, respectively (Figure 4). This attenuation in the reduction signal due to the incorporation of perturbations to the π-stack support the assignment of the electrochemical signal from EndoIII observed on closely packed DNA films being mediated by DNA CT. Conversely, when the same set of DNA substrates was compared using loosely packed DNA monolayers, there was no significant difference in the reduction signal observed with the introduction of these perturbations. The loosely packed DNA monolayers of WM, TC mismatched, and Ab DNA produced signal sizes of 45 ± 0.3 nA, 42 ± 1 nA, and 44 ± 1 nA respectively, which yield a p-value > 0.05 when compared using a one-tailed t-test, do not display statistically significant signal attenuation as compared to EndoIII bound to the closely packed DNA monolayer. This lack of signal attenuation with the incorporation of perturbation to the π-stack indicates that the DNA-bound signal of EndoIII is not mediated by electron transfer through the π-stack, in loosely packed DNA monolayers.

Kinetics of EndoIII reduction

The kinetics of EndoIII reduction was assessed on these two different dsDNA morphologies to explore further the mechanistic differences in the electron transfer pathways. In addition to the peak splitting, the EndoIII reduction on loosely and closely packed DNA monolayers was found to differ in the signal accumulation both as a function of scan rate as well as incubation time. For a diffusion rate-limited process this signal accumulation increases linearly as a function of the square root of the scan rate (34). The [4Fe-4S] cluster signal of EndoIII was measured over 10 different scan rates ranging from 10 mV/s to 200 mV/s on both loosely and closely packed dsDNA films and plotted as a function of the square root of the scan rate, $\nu^{1/2}$ (Figure 5). In the case of loosely packed dsDNA films, the current was found to be linear with respect to $\nu^{1/2}$, as previously established for the diffusion rate-limited reduction of DNA-bound [4Fe-4S] cluster proteins on this dsDNA film morphology (24). The same protein solution, on the same multiplexed chip, displayed nonlinear behavior on closely packed dsDNA films. More quantitative approaches for determining the rate of electron transfer, such as the Laviron analysis, were not possible due to the degree of heterogeneity of the observed electrochemical signals. However, the total signal accumulation for the reduction of EndoIII as a function of time on both these dsDNA film

NIH-PA Author Manuscript

NIH-PA Author Manuscript

NIH-PA Author Manuscript

morphologies displayed the same trend; loosely versus closely packed dsDNA films accumulated signal linearly and nonlinearly respectively, over time (Figure S2). This further supports the finding that only the signal observed on the loosely packed dsDNA films is limited by diffusion.

Multiplexed characterization of DNA CT proficiency

Since the electrochemical signal for the [4Fe-4S] cluster of EndoIII is generated primarily via DNA CT on closely packed dsDNA films, the DNA CT proficiency of a known disease-related mutant, Y82A, was compared to that of wild type EndoIII using this morphology. The Y82A mutant of EndoIII has previously been shown to be DNA CT deficient compared to wild type EndoIII using individual DNA-modified electrodes (21, 22). The DNA CT deficiency has been attributed to disruptions in the electron transport pathway from the DNA π–stack to the [4Fe-4S] cluster due to mutation of the aromatic tyrosine residue, located in close proximity to the π–stack based on the crystal structure of the wild type protein bound to DNA (36). The quantification of the extent of DNA CT proficiency for [4Fe-4S] cluster proteins has proven to be challenging due to the variability between individual DNA-modified electrodes.

Multiplexed characterization of the wild type (WT) and Y82A mutant EndoIII allows for a more quantitative comparison of the extent of coupling with the DNA-modified electrode. Multiplexed chips were assembled with half well-matched and half TC-mismatched closely packed dsDNA films. Orthogonally, WT and Y82A EndoIII were added to two quadrants each, such that each protein was incubated on both well matched and TC-mismatch DNA-modified electrodes (Figure 6). Samples of equal protein concentration were prepared based on the absorption at 410 nm, reflecting the [4Fe-4S] cluster concentration for each protein (~ 70 μM). Using this multiplexed configuration, the reduction of the [4Fe-4S] cluster in both WT and Y82A mutant EndoIII, was confirmed to have been generated via DNA CT, since both proteins displayed signal attenuation (23 ± 3 %) upon introducing a TC mismatch. Furthermore, the signal from Y82A was 72 ± 5 % attenuated compared to that of wild type EndoIII. Taken together with the attenuation upon mismatch incorporation, the observation of decreased DNA-mediated signal intensity verifies that the Y82A mutation results in a deficiency in DNA CT. Circular dichroism (CD) thermal denaturation confirmed that the stability of the protein fold was relatively unaltered upon introducing the Y82A mutation (Figure 6). Upon fitting the thermal denaturation curves to a 2-state unfolding model (32), melting temperatures for Y82A and WT EndoIII were found to be 49.2 ± 0.3 °C and 48.5 ± 0.3 °C respectively.

Direct comparison of electrostatic EndoIII mutants

Finally, the multiplexed DNA-modified electrodes were harnessed for the characterization of a new family of EndoIII mutants relative to wild type protein. In designing this new family of EndoIII mutants, only residues that were unlikely to cause significant changes in the DNA-binding affinity of EndoIII were chosen (37). The glycosylase activity of these mutants was verified to be equal to that of wild type protein (Figure S3), so that the observed electrochemical differences cannot be attributed to deficiencies in DNA binding. The Y205H, K208E and E200K EndoIII mutations investigated were originally designed to explore a possible shift in the mid-point potential of the [4Fe-4S] cluster, since these mutations alter the electrostatics surrounding the cluster. However, as can be seen in Figure 7, when compared in parallel on a single multiplexed chip on a closely packed dsDNA film, the mid-point potential of all the mutants are not found to be statistically different, ± 10 mV of the WT protein (Figure 7). Likely, the electrostatic effects of the DNA polyanion along with the associated counter ions mitigate any effects of local electrostatic changes of nearby peptides.

NIH-PA Author Manuscript

NIH-PA Author Manuscript

NIH-PA Author Manuscript

Interestingly, despite the lack of difference in mid-point potential, large differences in signal intensity between the mutants relative to WT were observed when the electrochemistry of the proteins was assayed at equivalent concentrations based on the absorbance of the [4Fe-4S] cluster at 410 nm, which are statistically significant with 95% confidence based on a two-tailed t-test. E200K yields a reductive current of 14.8 ± 0.3 nA in the cyclic voltammaogram, and is seen to be CT-deficient relative to WT EndoIII which displays a current intensity of 24.4 ± 0.8 nA. In contrast, K208E and Y205H exhibit significantly larger signals, 56.5 ± 2 nA and 118 ± 6 nA, respectively, relative to the WT protein.

To explore these significant differences, CD thermal denaturation experiments were performed. The melting temperature for the Y205H, K208E and E200K EndoIII as well as wild type protein (5 μM) are 45.0 ± 0.3 °C, 45.3 ± 0.3°C, 49.3 ± 0.3 °C, and 48.5 ± 0.3°C respectively (Figure 7). The denaturation temperature of these EndoIII mutants correlates with the electrochemical signal size. Those that show a thermal stability that is reduced relative to the wild type protein show a significantly higher signal size electrochemically. Conversely, E200K is slightly stabilized relative to the wild type protein, and displays an attenuated electrochemical signal. For all proteins, the signal initially grows with time and subsequently diminishes over extended incubation times. This signal decrease with time correlates with the thermal stability of the proteins; those proteins that are thermal destabilized diminish faster, while the signal persists for more stable proteins (Figure S4). Notably, the Y205H mutation, which is involved in hydrogen bonding to the [4Fe-4S] cluster, is found to be the most proficient in DNA CT, with a 5-fold larger signal than wild type, and the least stable mutant by both electrochemical measurements and CD thermal denaturation.

DISCUSSION

Multiplexed electrochemical analysis of EndoIII

In this study, the redox activity of the [4Fe-4S] cluster of EndoIII upon DNA binding was investigated using multiplexed DNA-modified electrodes. The utility of multiplexed analysis has previously been illustrated in using DNA-modified electrodes for the detection of biomarkers (3–11) as well as in performing sensitive measurements of DNA CT on long DNA duplexes (14). As there is growing interest in understanding of the redox properties of proteins containing [4Fe-4S] clusters that are involved in genome maintenance, the extension of multiplexed analysis has become essential to investigate these complex proteins and their subtle differences in redox behavior.

The electrochemical signal of EndoIII obtained using multiplexed DNA-modified electrodes was shown to be comparable to that seen using individual DNA-modified electrodes (20–22). Differences in peak potential and signal size are difficult to compare on individual electrodes given the variability in DNA-modified surfaces among experiments. The complexity of protein samples further amplifies this variability. Multiplexing removes the variability associated with protein preparation and surface modification. Specifically, multiplexing allows, with confidence, for a given protein to be examined in parallel across different DNA substrates or for many proteins to be compared on a given DNA-substrate. Thus, by harnessing this ability to probe in parallel for subtle differences in the electrochemical signal of EndoIII, effects of DNA substrate and morphology can be elucidated.

Mechanistic insights into EndoIII electrochemistry

Multiplexed analysis of the $3^{+}/2^{+}$ redox couple of EndoIII on differing DNA morphologies show subtle differences in the DNA-bound electrochemical signals. These differences in

NIH-PA Author Manuscript

NIH-PA Author Manuscript

NIH-PA Author Manuscript

electrochemistry result from differences in electron transfer pathways between the electrode and DNA-bound EndoIII that vary as a function of DNA film morphology. DNA-modified electrodes with single-stranded DNA, firstly, are found to function as an ideal control. Since EndoIII does not bind single-stranded DNA with high affinity, the single-stranded DNA does not serve as a means to increase the local concentration of EndoIII at the electrode surface. Moreover it appears that the negatively charged signal-stranded DNA serves as an effective passivation layer, preventing protein denaturation on the gold surface, a common occurrence for protein electrochemistry (38). Instead EndoIII appears to be electrochemically silent on these electrodes modified with single stranded DNA.

Secondly, the duplex DNA film morphology, established during electrode assembly, is demonstrated to be critical in dictating the predominant electron transfer pathway between the electrode surface and the [4Fe-4S] cluster of DNA-bound EndoIII. Differing electron transfer pathways to a single DNA-bound redox active moiety were previously characterized using DNA-modified electrodes with covalent redox active reporters (14, 35). In the case of a DNA-bound redox-active reporter, such as DNA-tethered methylene blue, it has been shown that the accessibility of the redox-active moiety to the electrode surface determines whether the predominant reduction mechanism is DNA CT or direct reduction by the surface of the electrode (35). In the case of the DNA-mediated reduction, we have established that the rate limiting step for the DNA-mediated reduction of distally bound redox active species is not DNA CT itself, but tunneling through the alkane thiol linkage to the electrode (39). The lateral charge diffusion through these DNA-modified films has also been established to be quite slow, negating the possibility of cross-talk throughout these films (40). The redox activity of EndoIII on DNA-modified electrodes assembled with closely packed DNA monolayers, with limited surface accessibility, display all the previously established hallmarks of a DNA-mediated reduction pathway, including increased peak splitting, signal broadening, sensitivity to perturbations, and non-diffusion rate limited kinetics. Conversely, the DNA-bound electrochemical signal from EndoIII on loosely packed DNA films, which have enhanced surface accessibility, display the opposite electrochemical behaviors that are characteristic of an electron transfer pathway that is not DNA-mediated. As both these signals involve reduction of *DNA-bound* EndoIII, the signals display only subtle differences. Only by using multiplexed analysis to investigate the electrochemistry of a single protein solution in parallel across differing DNA-modified electrodes are these two different electron transfer pathways cleanly distinguishable.

Electron transfer in EndoIII Mutants

Multiplexed analysis was demonstrated to be useful not only in the characterization of different electron transfer pathways from the electrode surface to the DNA-bound EndoIII, but also in comparing directly the electron transfer efficiencies of different EndoIII mutants. As proof-of-principle, the DNA CT proficiency of a known disease-related EndoIII mutant, Y82A, was electrochemically compared to wild type EndoIII. It has previously been established that introducing the Y82A mutation into EndoIII yields a functionally active protein that is DNA CT-deficient (21). Due to the proximity of this aromatic tyrosine residue to the DNA π-stack, the deficiencies in the electrochemical signal have been attributed to disrupting the electron transfer pathway between the DNA and [4Fe-4S] cluster (21). Our multiplexed experiment allowed for the validation of this result along with a more quantitative assessment of CT deficiency.

The mechanism of reduction for both wild type and Y82A EndoIII was shown to be DNA-mediated on the closely packed DNA films, since both proteins display the characteristic sensitivity to single base pair perturbations. The inherent DNA CT-deficiency of Y82A was characterized in parallel so that the difference in electrochemical efficiency of Y82A bound

NIH-PA Author Manuscript

NIH-PA Author Manuscript

NIH-PA Author Manuscript

to DNA compared to wild type can be conclusively attributed to decreased DNA CT proficiency. The degree of DNA CT deficiency quantified for this mutant was found to be twice as pronounced compared to previous measurements, given the overall decreased variability of the DNA-modified electrodes and, importantly, the decreased contributions from surface reduction of the [4Fe-4S] cluster due to the optimized DNA morphology.

Moreover, this multiplexed technology is sufficiently reliable to permit characterization of the effects on the electron transfer pathway of a new family of EndoIII mutations. This family was found to show significant differences in DNA CT efficiency, while displaying very similar DNA-bound reduction potentials for the $3^+/2^+$ redox couple of the [4Fe-4S]. Key to conclusively attributing differences, or lack thereof, observed in the mutant electrochemistry to changes in the electron transfer pathway through EndoIII was the ability to perform this comparison on identical gold surfaces, allowing for the geometry of electron transfer between the electrode and EndoIII to be held constant.

Previous work by Burgess and co-workers that focused on changing the electrostatics in *Azotobacter vinelandii* ferredoxin I resulted in large potential shifts; a single phenylalanine to histidine mutation caused a shift of over 200 mV for the [4Fe-4S] cluster while leaving overall protein structure unaffected (41). With the same aims, EndoIII mutations were prepared that invert the electrostatics of three residues within 4 Å of the [4Fe-4S] cluster that are oriented on the opposite face of the cluster relative to the DNA. Multiplexed analysis of these three different EndoIII mutants allowed for their simultaneous comparison to wild type EndoIII. The lack of distinguishable differences of the DNA-bound midpoint potentials for these electrostatic EndoIII mutants likely reflects the overwhelming contribution of polyanionic DNA, as DNA binding has already negatively shifts the reduction potential of EndoIII by approximately 200 mV (25). The strict consistency of the measured DNA-bound midpoint potentials likely further derives from the screening effect of counter-ions associated with the DNA, as well as from the broad, heterogeneous nature of the observed DNA-mediated signals.

As mentioned above, we have proposed a model where DNA repair proteins containing [4Fe-4S] clusters utilize DNA CT as a first step to localize to the vicinity of DNA damage (21). All of the proteins that we have investigated thus far have similar DNA-bound reduction potentials of approximately 80 mV vs. NHE (20). These results suggest that DNA-binding could be a mechanism that standardizes the reduction potentials of iron-sulfur cluster-containing DNA repair proteins once bound to DNA, allowing for efficient DNA-mediated electron self-exchange between repair proteins.

Unlike the Y82A mutation, these mutations were specifically designed to affect residues in close proximity to the [4Fe-4S] cluster but presumably without affecting the pathway for DNA-mediated electron transfer (Figure 8). Nonetheless, as seen in Figure 7, these changes unambiguously result in significant changes in the DNA CT efficiency. Multiplexed electrochemical characterization in conjunction with thermal denaturation circular dichroism experiments indicates that the differences in DNA CT efficiencies of these mutants are most likely caused by changes in the stability and solvent accessibility of the [4Fe-4S] cluster. Those proteins with decreased thermal stability show increased DNA CT yield compared to WT. Structured water molecules have been proposed to mediate efficient biological electron transfer in several intra- (42, 43) and intermolecular protein systems (44–46), generally by forming robust hydrogen-bonding pathways that increase electronic coupling between the donor and acceptor (47). We hypothesize that the destabilization we observe in Y205H and K208E EndoIII may result in the formation of a water pocket in EndoIII that would facilitate ET, as we have suggested previously for other destabilizing EndoIII mutations (22). In the case of E200K, which is slightly stabilized relative to wild type, substitution for a larger

NIH-PA Author Manuscript

NIH-PA Author Manuscript

NIH-PA Author Manuscript

lysine residue along the face of the cluster may instead screen the cluster from solvent and contribute to the observed CT deficiency. While the Y82A mutant is marginally stabilized compared to WT EndoIII, it is more significantly defective in DNA CT proficiency compared to E200K. Therefore, the extent the DNA CT deficiency of Y82A cannot be fully attributed to the change in stability and is thought to originate from directly disrupting the electron transfer pathway. Overall, it appears that differences in DNA CT proficiency can be caused both by altering the electron transfer pathway by removing aromatics and also by more indirectly modulating the electronic coupling of the cluster by changing protein stability and presumably solvent accessibility.

CONCLUSION

Multiplexed characterization of the DNA repair protein EndoIII bound to DNA provides new insights into the DNA-mediated reduction of this metalloprotein and the resolution of subtle electrochemical variations associated with DNA substrate and surface morphology. Multiplexed analysis leads to more reliable statistics as well as decreased surface variability and background contribution. The reduction of EndoIII is seen to be DNA-dependent, yet once bound to duplex DNA, there are two different pathways through which the electron transfer proceeds. The predominant mechanism for the reduction of the [4Fe-4S] cluster of EndoIII is shown to correlate with the surface accessibility of the protein, resulting in DNA-mediated reduction being observed only with closely packed DNA films. In addition to the electron transfer pathway between the electrode surface and EndoIII being characterized, the use of multiplexed analysis also allowed for the direct comparison of electron transfer pathways through the protein itself. The electrochemistry and stability of various EndoIII mutants was characterized, including a new family of mutations introducing electrostatic changes in close proximity to the [4Fe-4S] cluster. The stability of a given mutation was shown to correlate with the electrochemical yield, leading to the hypothesis that mutations not directly on the electron transfer pathway through the protein can alter the rate of electron transfer by affecting the solvation surrounding the [4Fe-4S] cluster. Most interestingly, this side-by-side quantitative comparison of varying electrostatics in the protein fold provides a demonstration of the dominance that DNA-binding elicits on the reduction potential of DNA repair proteins.

These multiplexed chips provide the needed flexibility and robustness to characterize the redox activity of emerging [4Fe-4S]-containing proteins that bind DNA. Multiplexed analysis will be integral in relating the function and redox activity of these DNA-binding proteins in order to establish roles for these critical redox active co-factors *in vivo*.

Supplementary Material

Refer to Web version on PubMed Central for supplementary material.

Acknowledgments

We are grateful for the financial support of the National Institute of Health (GM49216) and ONR (N00014-09-1-1117). A.R.A. was supported by the National Institute On Aging of the NIH on a pre-doctoral NRSA (F31AG040954). The authors also thank the Kavli Nanoscience Institute facilities and staff for help in streamlining the fabrication of multiplexed chips.

REFERENCES

1. Zheng G, Patolsky F, Cui Y, Wang UW, Lieber CM. Nature Biotechnol. 2005; 23:1294. [PubMed: 16170313]
2. Morrow TJ, Li M, Kim J, Mayer TS, Keating CD. Science. 2009; 323:352. [PubMed: 19150837]

NIH-PA Author Manuscript

NIH-PA Author Manuscript

NIH-PA Author Manuscript

3. Swensen JS, Xiao Y, Ferguson BS, Lubin AA, Lai RY, Heeger AJ, Plaxco KW, Soh HT. J. Am. Chem. Soc. 2009; 131:4262. [PubMed: 19271708]
4. Plaxco KW, Soh HT. Trends in Biotechnology. 2011; 29:1. [PubMed: 21106266]
5. Bonham AJ, Hsieh K, Ferguson BS, Vallee-Belisle A, Ricci F, Soh HT, Plaxco KW. J. Am. Chem. Soc. 2012; 134:3346. [PubMed: 22313286]
6. White RJ, Kallewaard HM, Hsieh W, Patterson AS, Kasehagen JB, Cash KJ, Uzawa T, Soh HT, Plaxco KW. Anal. Chem. 2012; 84:1098. [PubMed: 22145706]
7. Hsieh K, Patterson AS, Ferguson BS, Plaxco KW, Soh HT. Angew. Chem. Int. Ed. 2012; 51:4896.
8. Fang Z, Soleymani L, Pampalakis G, Yoshimoto M, Squire JA, Sargent EH, Kelley SO. ACS Nano. 2009; 10:3207. [PubMed: 19736919]
9. Vasilyeva E, Lam B, Fang Z, Minden MD, Sargent EH, Kelley SO. Angew. Chem. Int. Ed. 2011; 50:4137.
10. Lam B, Fang Z, Sargent EH, Kelley SO. Anal. Chem. 2012; 84:21. [PubMed: 22142422]
11. Das J, Cederquist KB, Zaragoza AA, Lee PE, Sargent EH, Kelley SO. Nat. Chem. 2012; 4:642. [PubMed: 22824896]
12. Pheeney CG, Guerra LF, Barton JK. Proc. Natl. Acad. Sci. 2012; 109:11528. [PubMed: 22733728]
13. Slinker JD, Muren NB, Gorodetsky AA, Barton JK. J. Am. Chem. Soc. 2010; 132:2769. [PubMed: 20131780]
14. Slinker JD, Muren NB, Renfrew SE, Barton JK. Nat. Chem. 2011; 3:228. [PubMed: 21336329]
15. Genereux JC, Barton JK. Chem. Rev. 2010; 110:1642. [PubMed: 20214403]
16. Murphy CJ, Arkin MR, Jenkins Y, Ghatlia ND, Bossmann SH, Turro NJ, Barton JK. Science. 1993; 262:1025. [PubMed: 7802858]
17. Wagenknecht, HA., editor. Charge Transfer in DNA:From Mechanism to Application. Weiheim: Wiley-VCH Verlag GmbH & Co KGaA; 2005.
18. Boon EM, Ceres DM, Drummond TG, Hill MG, Barton JK. Nat. Biotechnol. 2000; 18:1096. [PubMed: 11017050]
19. Boal AK, Barton JK. Bioconjugate Chem. 2005; 16:312.
20. Boal AK, Yavin E, Lukianova OA, O'Shea VL, David SS, Barton JK. Biochemistry. 2005; 44:8397. [PubMed: 15938629]
21. Boal AK, Genereux JC, Sontz PA, Gralnick JA, Newman DK, Barton JK. Proc. Natl. Acad. Sci. U.S.A. 2009; 106:15237. [PubMed: 19720997]
22. Romano CA, Sontz PA, Barton JK. Biochemistry. 2011; 50:6133. [PubMed: 21651304]
23. Lee PE, Demple B, Barton JK. Proc. Natl. Acad. Sci. 2009; 106:13164. [PubMed: 19651620]
24. Mui TP, Fuss JO, Ishida JP, Tainer JA, Barton JK. J. Am. Chem. Soc. 2011; 133:16378. [PubMed: 21939244]
25. Gorodetsky AA, Boal AK, Barton JK. J. Am. Chem. Soc. 2006; 128:12082. [PubMed: 16967954]
26. Wu Y, Suhasini AN, Brosh RM Jr. Cell. Mol. Life Sci. 2009; 66:1209. [PubMed: 19099189]
27. Vaithiyalingam S, Warren EM, Eichman BF, Chazin WJ. Proc. Natl. Acad. Sci. U.S.A. 2010; 107:13684. [PubMed: 20643958]
28. White MF, Dillingham MS. Current Opinion in Structural Biol. 2012; 22:94.
29. Wu Y, Brosh RM Jr. Nucleic Acids Research. 2012; 10:1.
30. Sontz PA, Mui TP, Fuss JO, Tainer JA, Barton JK. Proc. Natl. Acad. Sci. 2012; 109:1856. [PubMed: 22308447]
31. Cunningham RP, Asahara H, Bank JF, Scholes CP, Salerno JC, Surerus K, Münck E, McCracken J, Peisach J, Emptage MH. Biochemistry. 1989; 28:4450. [PubMed: 2548577]
32. Koepf EK, Petrassi HM, Sudol M, Kelly JW. Protein Sci. 1999; 8:841. [PubMed: 10211830]
33. Lapierre MA, O'Keefe M, Taft BJ, Kelley SO. Anal. Chem. 2003; 75:6327. [PubMed: 14616017]
34. Bard, AJ.; Faulkner, LR. Electrochemical Methods—Fundamental and Application. 2nd ed.. New York: John Wiley&Sons; 2000. p. 580-631.
35. Pheeney CG, Barton JK. Langmuir. 2012; 28:7063. [PubMed: 22512327]
36. Fromme JC, Verdine GL. EMBO J. 2003; 22:3461. [PubMed: 12840008]

NIH-PA Author Manuscript

NIH-PA Author Manuscript

NIH-PA Author Manuscript

37. Thayer MM, Ahern H, Xing D, Cunningham RP, Tainer JA. EMBO J. 1995; 14:4108. No residues in the conserved DNA-binding FCL motif, residues Thr186 – Cys194, were mutated. [PubMed: 7664751]

38. Zhang J, Chi Q, Hansen AG, Jensen PS, Salvatore P, Ulstrup J. FEBS Letters. 2012; 586:526. [PubMed: 22024483]

39. Drummond TG, Hill MG, Barton JK. J. Am. Chem. Soc. 2004; 126:15010. [PubMed: 15547981]

40. Kelley SO, Jackson NM, Hill MG, Barton JK. Angew. Chem. Int. Ed. 1999; 38:941.

41. Chen K, Bonagura CA, Tilley GJ, McEvoy JP, Jung YS, Armstrong FA, Stout CD, Burgess BK. Nature Struct. Biol. 2002; 9:188. [PubMed: 11875515]

42. Francisco WA, Wille G, Smith AJ, Merkler DJ, Klinman JP. J. Am. Chem. Soc. 2004; 126:13168. [PubMed: 15479039]

43. Casimiro DR, Richards JH, Winkler JR, Gray HB. J. Phys. Chem. 1993; 97:13073.

44. Tezcan FA, Crane BR, Winkler JR, Gray HB. Proc. Natl. Acad. Sci. U.S.A. 2001; 98:5002. [PubMed: 11296248]

45. van Amsterdam IMC, Ubbink M, Einsle O, Messerschmidt A, Merli A, Cavazzini D, Rossi GL, Canters GW. Nat. Struct. Biol. 2002; 9:48. [PubMed: 11740504]

46. Miyashita O, Okamura MY, Onuchic JN. Proc. Natl. Acad.Sci. U.S.A. 2005; 102:3558. [PubMed: 15738426]

47. Lin J, Balabin IA, Beratan DN. Science. 2005; 310:1311. [PubMed: 16311331]

NIH-PA Author Manuscript
NIH-PA Author Manuscript
NIH-PA Author Manuscript

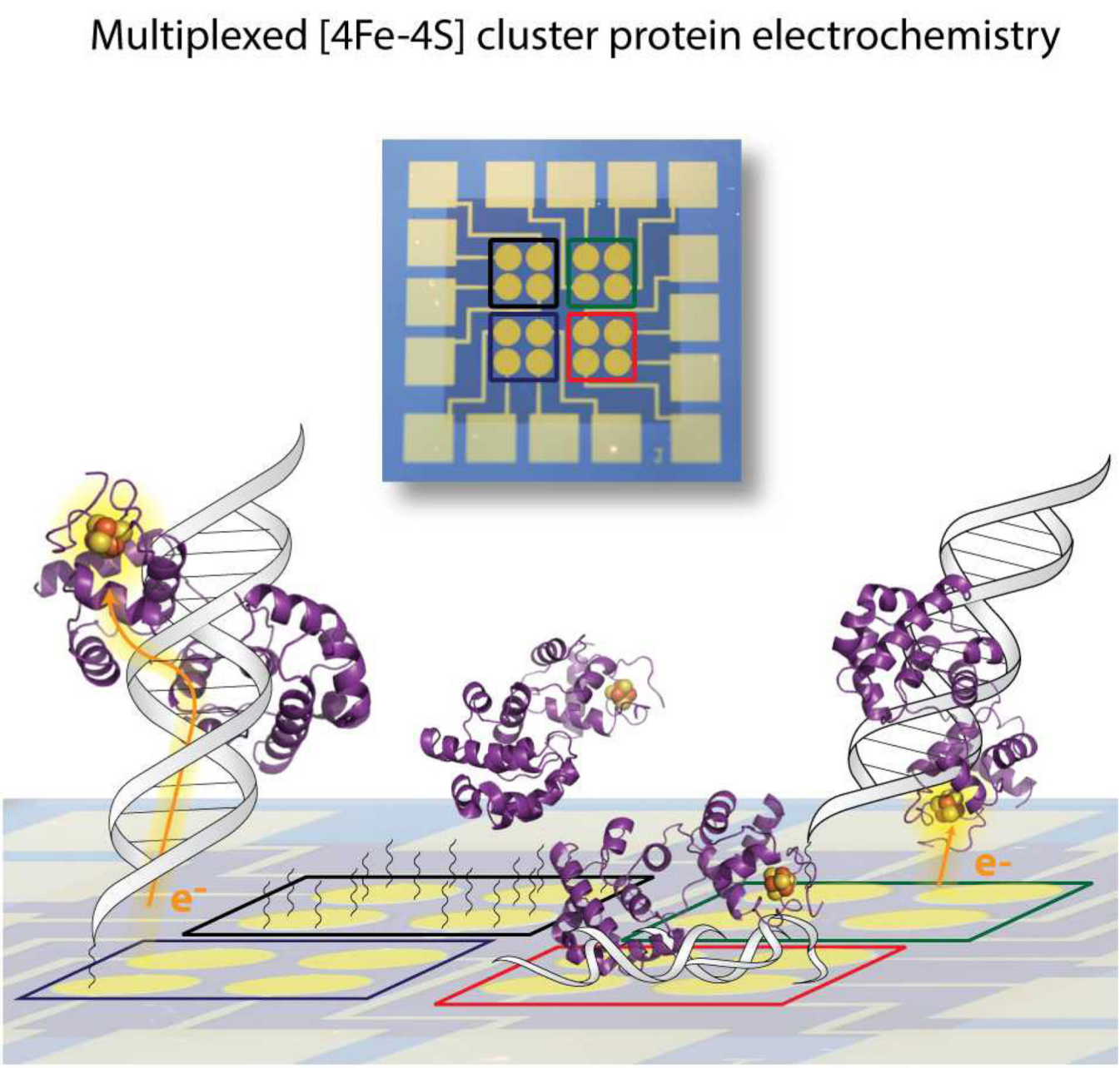

Figure 1.
Schematic depicting the versatility of multiplexed analysis for the investigation of metalloprotein electrochemistry. Our multiplexed devices are composed of 16 electrodes that are divisible into 4 separate quadrants of 4 electrodes, having the capability of producing 4 distinct experimental conditions on a single Au surface. This assembly allows for facile comparisons of the electrochemical signal from various DNA-bound proteins across varying DNA substrates and morphologies.

NIH-PA Author Manuscript
NIH-PA Author Manuscript
NIH-PA Author Manuscript

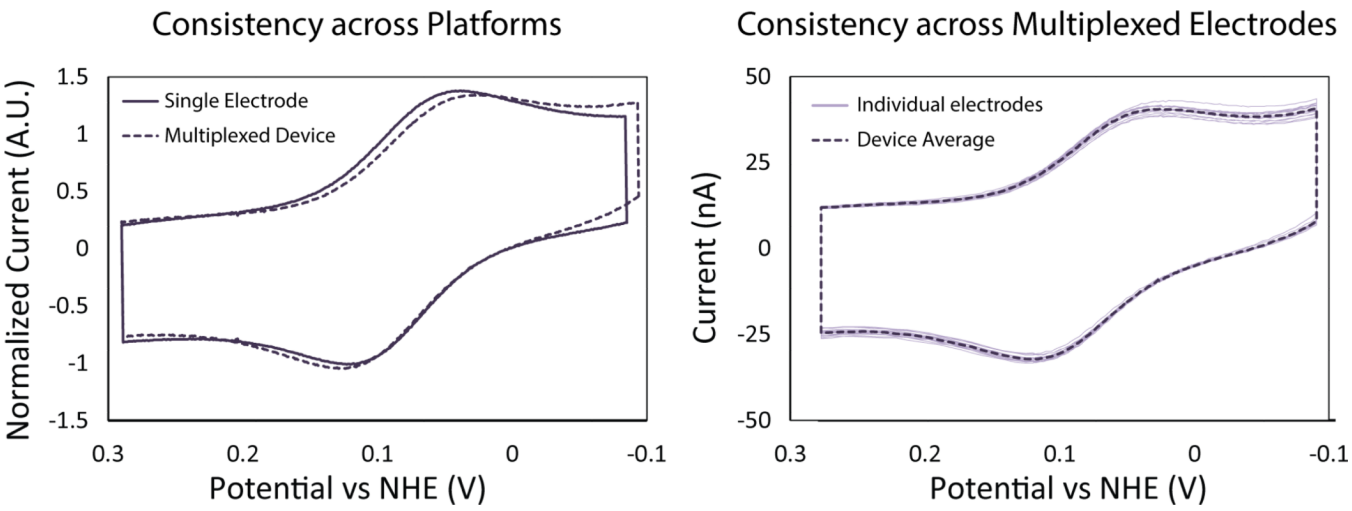

Figure 2.

Consistency of DNA-modified electrodes. (*Left*) The signals generated after incubation of loosely packed DNA-modified electrodes with EndoIII (30 μM) in phosphate buffer (20 mM sodium phosphate, 100 mM NaCl, 0.5 mM EDTA, 20 % glycerol, pH 7.4) were used to directly compared the single (solid) and multiplexed (dashed) electrochemical assemblies. The cyclic voltammetry (scan rate = 100 mV/s) was normalized, based on the capacitance at 0.3 mV vs NHE, so relative signal sizes could be compared across platforms. (*Right*) The variability of the EndoIII signal, under the same conditions, across all 16 electrodes (light solid line) of a single multiplexed device was within 3.5% of the average CV for the device (dark dashed line).

NIH-PA Author Manuscript

NIH-PA Author Manuscript

NIH-PA Author Manuscript

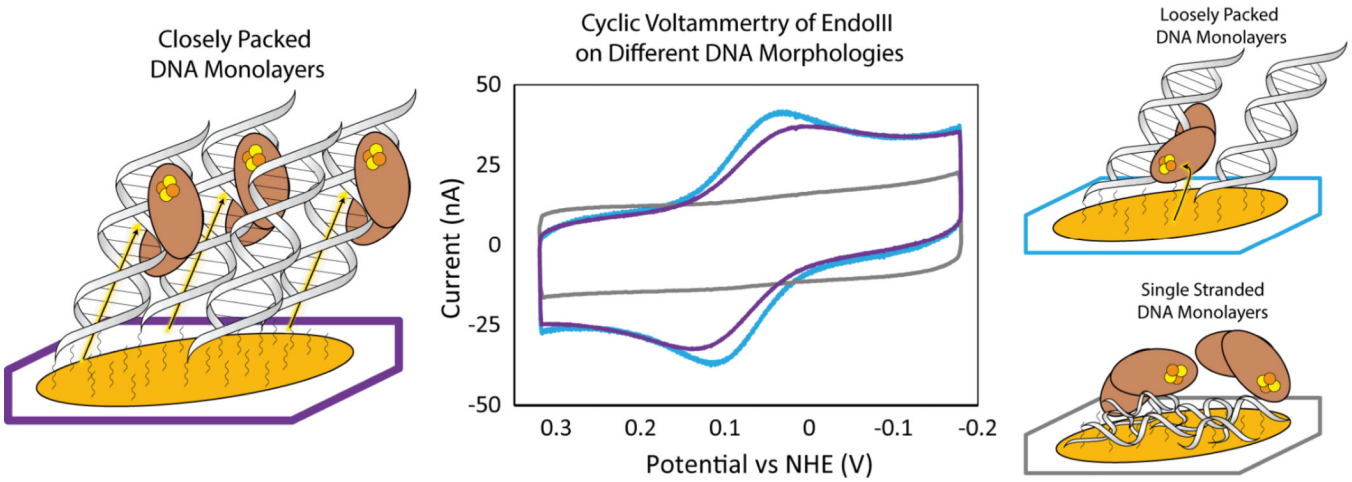

Figure 3.

The electrochemistry of EndoIII on DNA-modified electrodes was determined as a function of the underlying DNA film morphology. DNA monolayers were allowed to self-assemble over 16–24 hours either with or without 100 mM $MgCl_2$ to form either closely (purple) or loosely (blue) packed DNA monolayers. All morphologies were directly compared on the same multiplexed device so the differences in the EndoIII (60 μM) redox signal could be resolved. Cyclic voltammetry scans (scan rate = 100 mV/s) were compared in phosphate buffer (20 mM sodium phosphate, 100 mM NaCl, 0.5 mM EDTA, 20 % glycerol, pH 7.4) and the peak splitting and signal size were both quantified. Single-stranded DNA monolayers (grey) were prepared and shown to not produce a DNA-bound EndoIII signal.

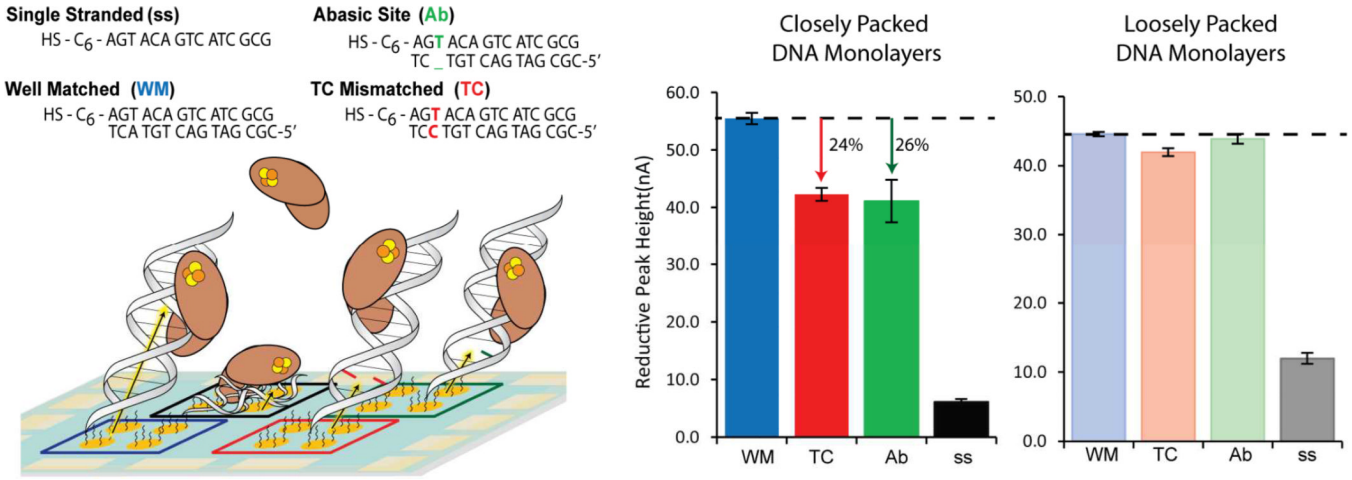

Figure 4.

The degree of signal attenuation induced by a single perturbation to the π-stack, for both closely and loosely packed DNA monolayers was investigated. (*Left*) Schematic of multiplexed devices prepared with well-matched (blue), TC mismatched (red), and abasic site (green) duplex DNA, and a single-stranded control (black).The sequences are indicated above. (*Right*) The reductive signals from DNA-bound EndoIII in phosphate buffer (20 mM sodium phosphate, 100 mM NaCl, 0.5 mM EDTA, 20 % glycerol, pH 7.4) were quantified for DNA monolayers assembled in both the presence (dark) and absence (light) of 100 mM $MgCl_2$ yielding closely and loosely packed DNA, respectively. The percent signal attenuations of the TC mismatch and abasic site were determined based on the average signal size, across all four electrodes in a quadrant, compared to that of well-matched DNA. The signals generated from closely packed DNA-films displayed distinct attenuation upon introducing either a mismatch or abasic site, while the signals from loosely packed DNA-films did not display this sequence dependence.

NIH-PA Author Manuscript
NIH-PA Author Manuscript
NIH-PA Author Manuscript

NIH-PA Author Manuscript
NIH-PA Author Manuscript
NIH-PA Author Manuscript

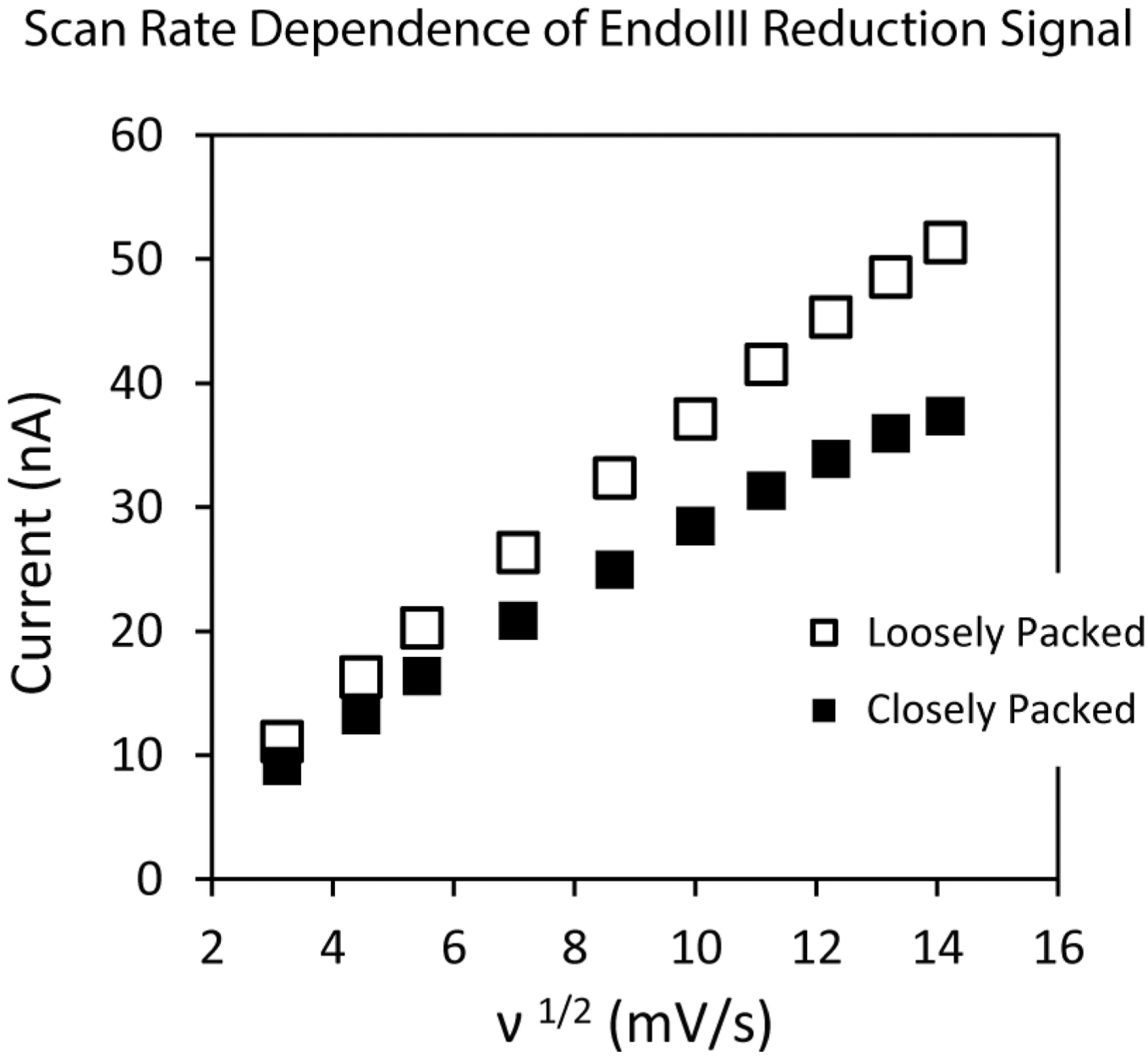

Figure 5.

Kinetic analysis of the signal generated from EndoIII on differing DNA film morphologies is indicated. Cyclic voltammetry (scan rates ranging from 10 mV/s to 200 mV/s) of EndoIII were obtained in phosphate buffer (20 mM sodium phosphate, 100 mM NaCl, 0.5 mM EDTA, 20 % glycerol, pH 7.4) for both closely (solid) and loosely (outlined) packed DNA monolayers. The reductive peak height for both morphologies, on the same multiplexed device, was quantified and plotted as a function of the square root of the scan rate, $v^{½}$. The non-linearity of the signal from closely packed DNA films indicates that the signal is not diffusion rate limited.

NIH-PA Author Manuscript
NIH-PA Author Manuscript
NIH-PA Author Manuscript

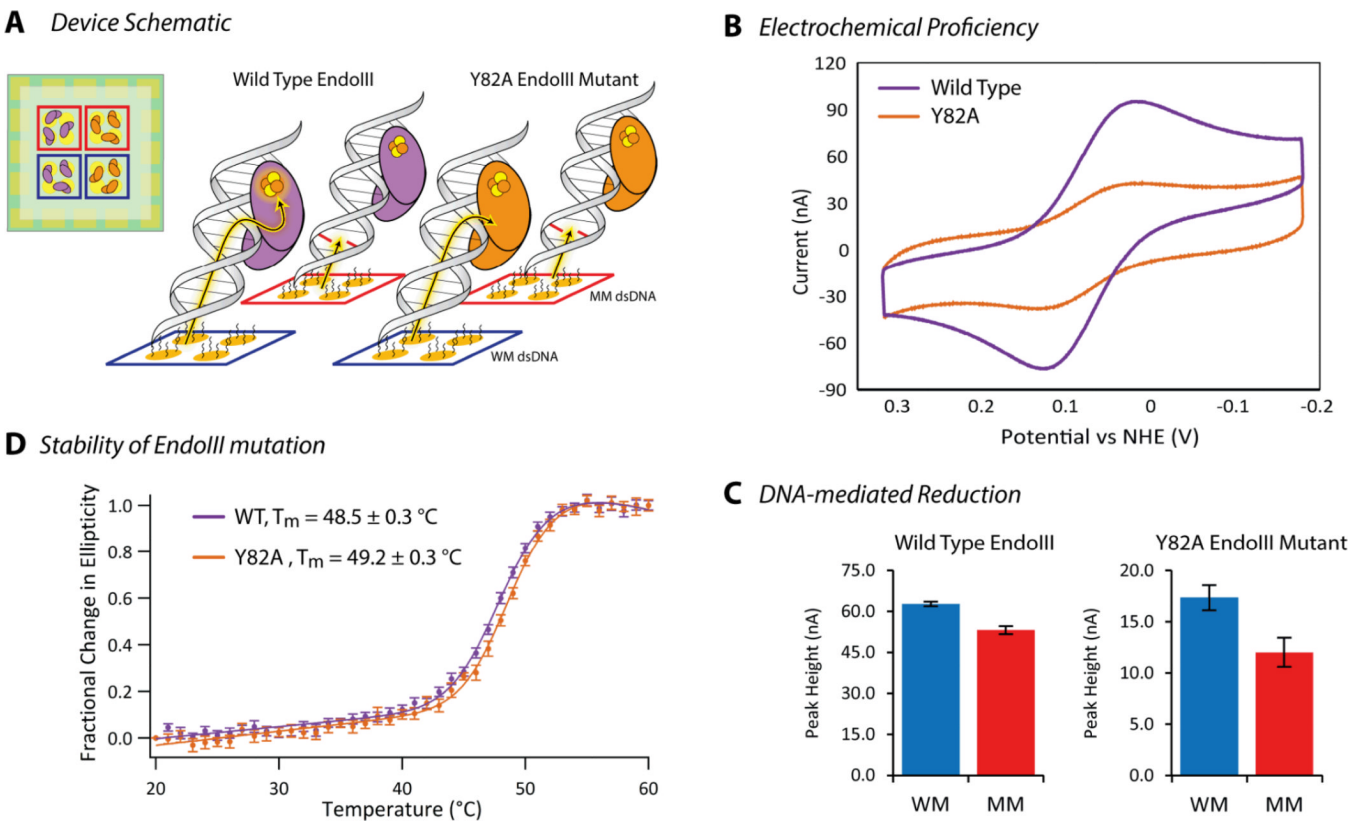

Figure 6.

Comparison of the electrochemical properties and stability of wild type EndoIII and a Y82A mutant. (*A*) Multiplexed electrode assembly schematic where electrodes are assembled with 100 mM $MgCl_2$, with either well-matched (blue) or TC mismatched (red) duplex DNA, and then incubated with either wild type (purple) or Y82A (orange) EndoIII (70 μM, based on absorbance at 410 nm). (*B*) Cyclic voltammetry (scan rate = 100 mV/s) in phosphate buffer (20 mM sodium phosphate, 100 mM NaCl, 0.5 mM EDTA, 20 % glycerol, pH 7.4) are indicated for both wild type and Y82A EndoIII on closely packed, well-matched DNA monolayers. (*C*) The reductive signal upon introducing a TC mismatch (red) compared to well-matched (blue) validates the mechanism of reduction to be DNA-mediated for both proteins. (*D*) Circular dichroism thermal denaturation (5 μM protein) validates that the Y82A mutation does not significantly alter the stability of the protein.

NIH-PA Author Manuscript
NIH-PA Author Manuscript
NIH-PA Author Manuscript

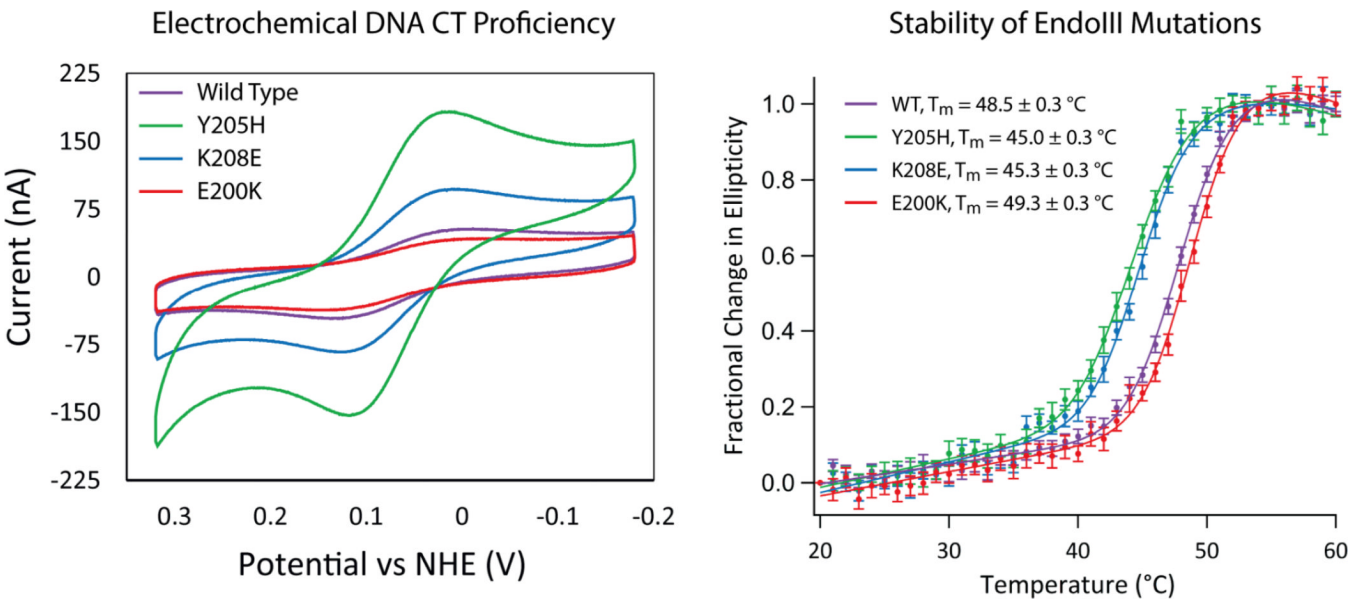

Figure 7.

Electrochemical and stability comparison of a new family of electrostatic EndoIII mutations, Y205H (green), K208E (blue), and E200K (red), with wild type EndoIII (purple). (*Left*) Cyclic voltammetry (scan rate = 100 mV/s) in phosphate buffer (20 mM sodium phosphate, 100 mM NaCl, 0.5 mM EDTA, 20 % glycerol, pH 7.4) is displayed for all four proteins on closely packed, (assembled with 100 mM Mg Cl_2) well-matched DNA monolayers. Protein samples had equivalent concentrations of [4Fe-4S] (70 μM based on the 410 nm absorbance). (*Right*) Circular dichroism thermal denaturation (5 μM protein) was performed to correlate the altered electronic coupling of these mutations in close proximity of the [4Fe-4S] cluster with the differential stability of the proteins.

NIH-PA Author Manuscript
NIH-PA Author Manuscript
NIH-PA Author Manuscript

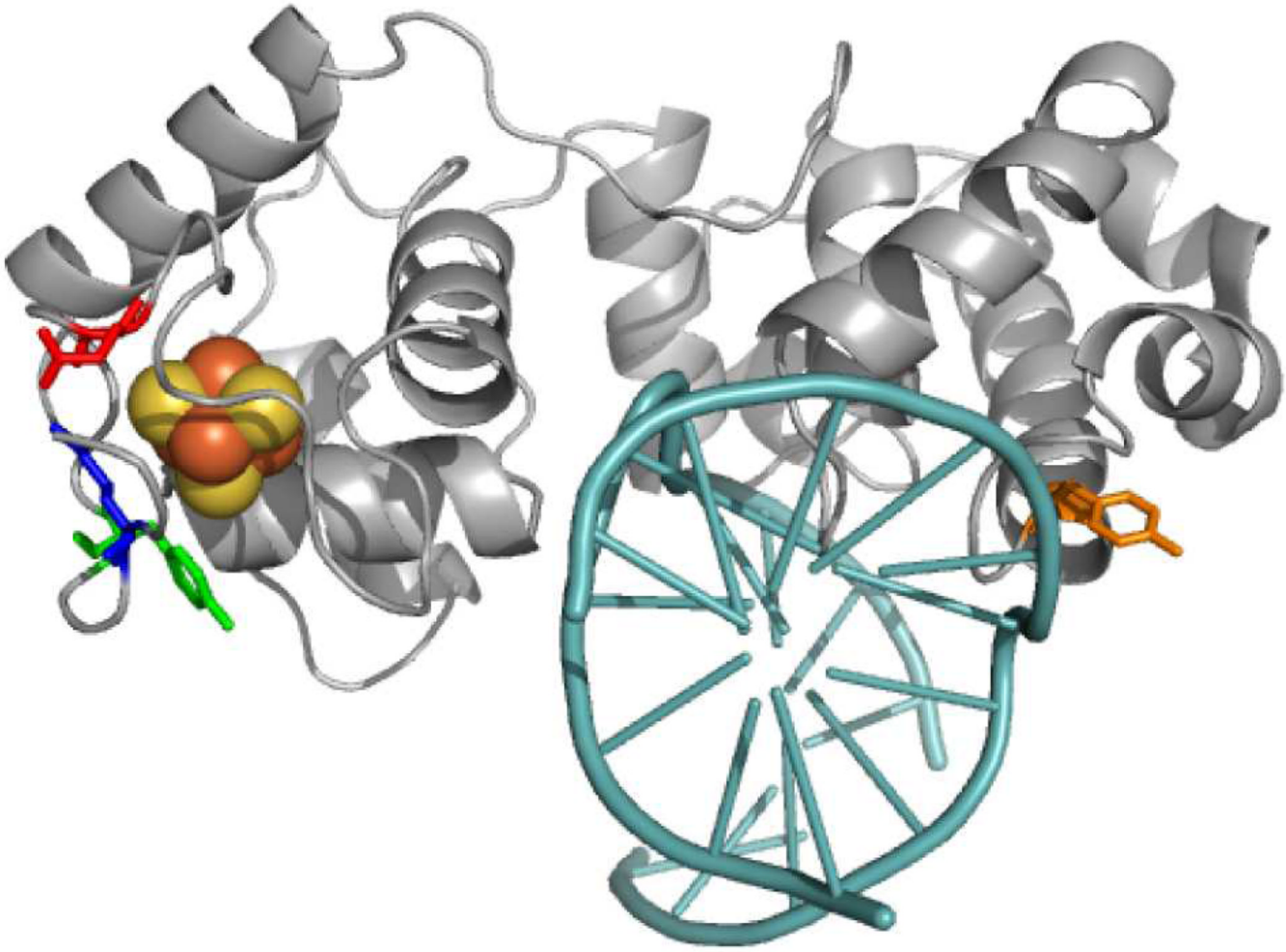

Figure 8.
Crystal structure of EndoIII with the location of mutants shown relative to the DNA (cyan) and [4Fe-4S] cluster: Y205 (green), K208 (blue), E200 (red), and Y82 (orange). PDB: 2ABK with DNA from 1ORN.